03,08

The mechanism of resistive switching in memristors based on organometallic perovskites

© N.I. Alekseev[1,2], A.N. Aleshin[1]

[1] Ioffe Institute,
St. Petersburg, Russia
[2] St. Petersburg State Electrotechnical University „LETI"
St. Petersburg, Russia

E-mail: NIAlekseyev@yandex.ru

Received December 29, 2023
Revised February 8, 2024
Accepted February 11, 2024

The mechanisms of current transfer in a film of organometallic perovskite are analyzed. It is shown that the current is mainly determined by the transfer of halogen ions and halogen vacancies, and the volt-ampere characteristics (VAC) of the metal|perovskite|metal structure should be close to exponential. The experimental VAC obtained up to the moment of resistive switching is well described by the model of electron transfer along the boundaries of perovskite grains. The possibility of a specific switching mechanism associated with the splitting of the film volume into vortex cells of the Benard cell type is also shown. An assessment of the possible size of such cells and the threshold of their formation is made.

Keywords: electrical conductivity, dissipative structures, physical model.

DOI: 10.61011/PSS.2024.03.57938.278

1. Introduction

Memristors (ReRAM, resistive random-access memory) are one of the candidate types of universal computer memory combining the advantages of random-access memory, hard drives, and flash memory. The operation of ReRAM relies on resistive switching, which is the effect of reversible variation of the resistance of a dielectric layer (or memory medium) in a metal|insulator|metal (semiconductor) structure under the application of voltage of a certain magnitude and polarity. Memristors typically have two (LR and HR, low- and high-resistance) states, although states with an intermediate resistance may also be present [1]. The processes governing resistive switching (RS) depend largely on materials of the memory medium and electrodes. Specifically, it is assumed that ions of the electrode material or oxygen vacancies play a leading part when an oxide medium is used [2,3].

Changes induced by the motion of these vacancies establish paths for electron transport modification (such as the formation of conductive filaments with a high electronic conductivity or alteration of the Schottky barrier for electrons) in the memory medium. At the same time, the densities of vacancies and majority carriers (electrons) in oxide memristors remain at the same and fairly low level: $(10^{10}-10^{13})\,\mathrm{cm}^{-3}$.

The most typical basic current transport mechanisms in such a medium outside of switching points are the propagation of electrons through a space charge region, hopping conduction along electron traps, etc.

Apparently, memristors based on inorganic perovskites (structures similar to $CsPbI_3$ and $CsPbBr_3$) fit the same mold. The interest in perovskites, both organic and hybrid organometallic ones, stems from their specific features making them well-suited for application in solar cells (SCs):

– high absorption of visible solar radiation within thin films that are relatively cheap to produce;

– low exciton binding energy, which is important for electron–hole separation upon radiation absorption;

– long diffusion length of carriers, which allows them to propagate over large distances within an SC; and

– several other features.

The possibility of switching the state of a perovskite-based memristive system via illumination encourages one to examine optoelectronic and memristive properties within a single approach.

Some of these properties are even more pronounced in hybrid perovskites of the $(MA)PbX_3$ type, where X is a halogen (in most cases, iodine or bromine) and MA is a methylammonium CH_3NH_3 molecule. The lattice of $(MA)PbX_3$ consists of cubic lattices of singly charged MA cations and lead ions inserted into each other and a tetrahedral lattice of halogen ions with the centers of tetrahedra located at lead ions (Figure 1).

Atoms at oxygen−halogen and metal−MA sites in this lattice get substituted relative to inorganic perovskite, inducing a change in material properties. The present study is aimed at constructing a physical model that characterizes the influence of these properties on an elementary memristive structure with hybrid perovskite (metal|$(MA)PbX_3$|metal). Specifically, the qualitative shape

of stationary VACs in the write mode and possible RS mechanisms in this structure are examined. In what follows, hybrid perovskite is sometimes referred to as HP for brevity.

2. Results and discussion

Compared to inorganic perovskite, HP has a major „anomalous" feature in its extremely low densities of „common" carriers (electrons and holes) at the level of $(10^9-10^{13})\,\mathrm{cm}^{-3}$ that are coupled with very low energies of lattice defect formation (and, consequently, correspondingly high densities of dominant ions at the level of $(10^{18}-10^{20})\,\mathrm{cm}^{-3}$ [4,5]). Similar carrier densities have earlier been observed only in multicomponent materials processed in a solution (e. g., Cu_2ZnSnS_4).

A Schottky defect [6] (formation of stoichiometric amounts of anion and cation vacancies that may be distributed randomly in a crystal) is the dominant type of defects in inorganic perovskites. The same defect is also a convenient base type for hybrid $(MA)PbX_3$ systems. However, one of the reactions forming a Schottky defect and associated with the migration of a halogen ion along a diagonal in a halogen tetrahedron (Figure 1) then has a much lower activation barrier E_a than the migration of MA and lead, since it does not require rotating octahedral cells [4] or shifting neighboring atoms further apart. According to [4], barrier E_a is 0.58 eV, which is much lower than the values of 0.84 eV for MA migration and 2.3 eV for migration of a lead ion. Even lower migration activation energies have been obtained in earlier calculation [5], where E_a for halogen was just around 0.2 eV.

In [4], the energy barriers were estimated via chronophotoampereometry measurements; in addition, the authors estimated the densities of halogen ions and positive vacancies induced by them at $(10^{18}-10^{19})\,\mathrm{cm}^{-3}$ (in what follows, these are simply called ions and vacancies for brevity). The indicated density value also corresponds to a rough Saha estimate with an activation energy of 0.6 eV at room temperature (RT, 300 K) obtained by associating the escape of a halogen ion from a lattice site with thermal ionization of an atom, the initial neutral cell with this atom, a halogen ion with an electron, and the cell left by halogen (i. e., vacancy) with an ionized atom.

The origin of an anomalously high density was discussed in [5] at the level of crystal chemistry of a hybrid cell, and we do not cover this here. Specifically, it was demonstrated that produced point defects minimize the free energy of a crystal without generating „traditional" carriers (electrons and holes). The authors of recent study [7] have provided a more advanced insight into this issue.

A low energy of activation of ions and vacancies translates into a very high mobility of halogens μ_X (at the level of $20\,\mathrm{cm}^2/(\mathrm{V}\cdot\mathrm{s})$ [4,5,8]) and a very long diffusion length of carriers in high-quality hybrid perovskite thin films ($>1\,\mu$m). This μ_X estimate appears to be reasonable, although it may differ from the estimate following from the

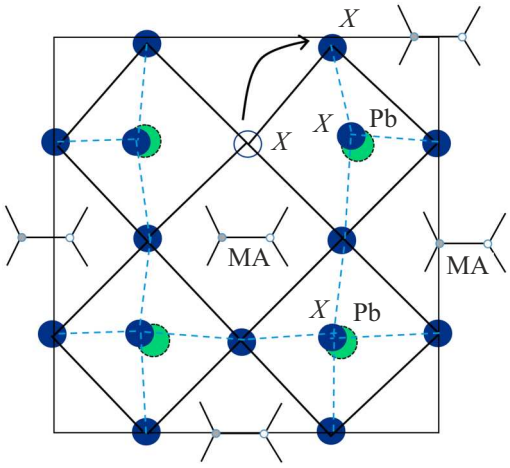

Figure 1. Main motif of migration of lattice components in $(MA)PbX_3$ perovskites is the motion of halogen X ions along the faces of a halogen tetrahedron. Each tetrahedron is marked by corner halogen ions that lie above the picture plane and cover partially the ions of lead at the center of every tetrahedron.

fundamental relation of chemical kinetics with an activation barrier of transition to a neighboring cell of 0.6 eV and transition length Δ equal to the cell size of perovskite (i. e., approximately 6 Å). The resulting probability of ion transition between neighboring cells is then

$$w \approx \frac{T}{h}\frac{Q^*}{Q_0}\exp\left(-\frac{E_a}{T}\right)\left(\exp\left(\frac{F\Delta}{T}\right)-\exp\left(-\frac{F\Delta}{T}\right)\right)$$
$$\approx \frac{2F\Delta}{h}\exp\left(-\frac{E_a}{T}\right), \qquad (1)$$

where (Q^*/Q_0) is the ratio of partition functions in the initial and transition states and F is the electrical field; the difference between exponential functions factors in the mismatch of probabilities of ion escape from a cell along the field and opposite to it, and the drift velocity and the mobility are

$$v = w\frac{2F\Delta^2}{h}\exp\left(-\frac{E_a}{T}\right);$$
$$\mu_X = \frac{v}{F} \approx \frac{2\Delta^2}{h}\exp\left(-\frac{E_a}{T}\right). \qquad (2)$$

At $\Delta = 6$ Å, $E_a = 0.2$ eV, and RT and with no regard for the (Q^*/Q_0) ratio, $\mu_X = 10^{-3}\,\mathrm{cm}^2/(\mathrm{V}\cdot\mathrm{s})$ (i. e., is almost four orders of magnitude lower than the indicated value). However, the actual mobility should indeed decrease drastically due to the presence of numerous grain boundaries. That said, the advantage of ions and vacancies over electrons is so great that the results discussed below should remain unchanged. A combination of an anomalously high density of ions (and vacancies) N_{vac} and a low density of electrons and holes shapes the unusual physical pattern of conductivity and RS.

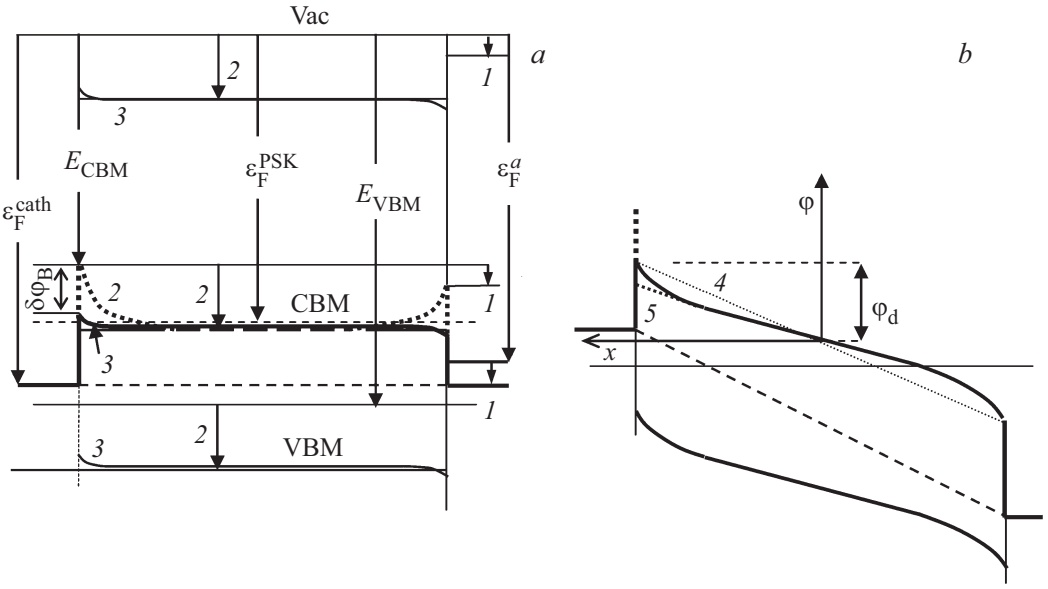

Figure 2. Changes in the electronic band structure of a metal|hybrid perovskite|metal system. E_{CBM}, E_{VBM} are the boundary energies of bands of perovskite not in contact with electrodes measured relative to vacuum. CBM, VBM are the positions of band boundaries after equilibration with electrodes. *a*) Electrodes are shorted. Arrows: *1* — shift of the vacuum level induced by alignment of Fermi levels of the cathode and the anode, *2* — positions of equilibrium band boundaries upon bringing perovskite into contact with electrodes under the condition of nominally immobile halogen ions and vacancies, and *3* — the same positions determined with account for migration of ions and vacancies. *b*) Voltage $V = 2\varphi_d$ relative to the cathode is applied to the anode. *4* — CBM boundary bending and *5* — narrowing of the bandgap and lowering of the CBM level at the cathode due to a high density of vacancies.

In addition to anomalously high μ_X and densities N_{vac}, this pattern is affected by a high entry barrier for electronic current from a metal cathode, which is set by the difference between work function ε_F^{cath} of the cathode and conducting band minimum (CBM) E_{CBM} of perovskite. The corresponding barrier in Figure 2, *a* for a gold cathode, $(MA)PbBr_3$ perovskite, and no migration of ions and vacancies is $5.1-3.36 = 1.74$ eV; as usual, the positions of band boundaries are characterized by positive values measured from the V_{ac} vacuum energy level along the energy scale directed downward). Since only positive voltage is discussed below and the type of metal electrodes is not specified, standard terms „cathode“ and „anode“ are used.

The densities of weak currents (below the milliampere level) typical of memristor operation are several orders of magnitude lower than the densities of field J_f and diffusion J_{diff} currents taken separately. Specifically, at a perovskite film thickness of 200 nm and a voltage of 0.5 V, the electrical field is $F \approx 2.5 \cdot 10^4$ V/cm, drift velocity $\mu_X F = 5 \cdot 10^5$ cm/s, and current density J_f at vacancy density $N_{vac} = 10^{18}$ cm^{-3} is at the level of 10^5 A/cm^2 (i. e., reaches $J_f \approx 10^2$ A/cm^2 even at μ_X being four orders of magnitude lower than $20\,\mathrm{cm}^2/(\mathrm{V}\cdot\mathrm{s})$). Therefore, perovskite as a whole may be regarded as an almost equilibrium plasma of halogen ions and vacancies, and the internal film volume may be called a gap (as in plasma physics). Current in this plasma is carried by the opposing motion of ions and vacancies. Their small difference corresponds to electronic current density J_e at the cathode interface. Electrons play a negligible role in this plasma, and the CBM profile adjusts to the potential profile shaped by ions and vacancies (this profile, the vacuum level, CBM, and the valence band maximum (VBM) are shown as profiles *3* in Figure 2, *a*; the initial positions of band boundaries are denoted as E_{CBM}, E_{VBM}). Therefore, changes in the band structure and the associated „electronic“ factors (specifically, electron propagation via traps within the gap) are not decisive for homogeneous perovskite. A Schottky barrier also assumes a different role: instead of controlling the current of electrons from a semiconductor to a metal [9], its lowering adjusts the entry metal–semiconductor barrier for electrons at the cathode interface.

Indeed, the solution of the Poisson equation for potential profile φ in the gap without electrons

$$\varphi'' = (T/r_D^2)[\exp(\varphi/T) - \exp(-\varphi/T)],$$

$$r_D^2 = T/(4\pi e^2 N_{vac}^{(0)}), \qquad (3)$$

(where φ is measured relative to the middle of the gap — Figure 2, *b*, $N_{vac}^{(0)}$ is the vacancy density in the middle of the gap, and r_D is the Debye radius, which is just 1 nm at a plasma density of 10^{18} cm^{-3}) after the first integration is given by

$$\frac{d\varphi}{dx} = \frac{T\sqrt{2}}{r_D}\left[\exp\left(\frac{\varphi}{T}\right) + \exp\left(-\frac{\varphi}{T}\right) - 2 + \frac{r_D^2\varphi_0'^2}{2T^2}\right]^{1/2}, \qquad (4)$$

(where axis x is directed from the middle of the gap to the cathode — Figure 2, b), φ_0' is the field in the middle of the gap, and

$$\varphi_0' \approx \frac{T\sqrt{2}}{r_{\mathrm{D}}}\,\frac{2\lambda}{\lambda^2-1},$$

where

$$\lambda = \exp\left(\frac{d\sqrt{2}}{r_{\mathrm{D}}} - 2\big(\exp(-1) - \exp(-\varphi_d/T)\big)\right) \qquad (5)$$

after the second integration over potential φ from 0 to cathode potential φ_d, which is 1/2 of the voltage across the gap (Figure 2, b). Since the mobilities of ions and vacancies are very high (although different), the potential curve is odd relative to the middle of the gap.

Owing to high densities of vacancies and halogens even in the middle of the gap $N_{\mathrm{vac}}^{(0)}$, the composition of a semiconductor in narrow near-electrode layers, where the density of vacancies (near the cathode) and ions (near the anode) increases as $\exp(\varphi_d/T)$, changes significantly. Even in equilibrium, when the cathode–anode potential drop (Figure 2, a) is induced just by a small difference between work functions $\varepsilon_{\mathrm{F}}^{\mathrm{cath}}$ and $\varepsilon_{\mathrm{F}}^{a}$, the CBM curve (*3*) near the cathode lies well below provisional curve *2* (and provisional shift of grain boundaries *2*) corresponding to immobile ions and vacancies. The electron current from the cathode entering a semiconductor is then

$$J_e = A_{\mathrm{Richardson}} \exp\big(-(\varepsilon_{\mathrm{F}}^{\mathrm{cath}} - E_{\mathrm{CBM}} - \delta\varphi_{\mathrm{B}})/T\big), \qquad (6)$$

where the Richardson pre-exponential factor is

$$A_{\mathrm{Richardson}} \approx \frac{3n_e v_{\mathrm{F}}^{\mathrm{cath}}}{16\pi}\left(\frac{T}{\varepsilon_{\mathrm{F}}^{\mathrm{cath}}}\right)^2 \approx 120\,\frac{A}{\mathrm{cm}^2\cdot\mathrm{K}}\,T^2\,[\mathrm{K}]$$

$$\underset{T=RT}{\approx} 1.1\cdot 10^7\,\frac{A}{\mathrm{cm}^2}, \qquad (7)$$

and $\delta\varphi_{\mathrm{B}} > 0$ is the difference between Schottky barriers with and without ion and vacancy migration. In the order of magnitude, $J_e \approx (10^{-9}-10^{-7})\,\mathrm{A/cm}^2$, which agrees with experimental data (Figure 3).

The CBM level at the anode lies above the Fermi energy; the anode interface is always an ohmic contact and is not considered below.

In the most general form, an increase in the positive charge of vacancies near the cathode implies, according to the Le Chatelier principle, that it should be easier for electrons in this region to reach the CB both from the valence band (VB) of perovskite and from the outside. This principle may be implemented via changes characterized in terms of a regular or amorphous semiconductor:

– bandgap (BG) narrowing,

– emergence of discrete electronic states within the BG near the CBM,

– penetration of „tails“ of the density of states (DoS) from the CB and the VB into the BG (this occurs in amorphous semiconductors, where tails correspond to localized states).

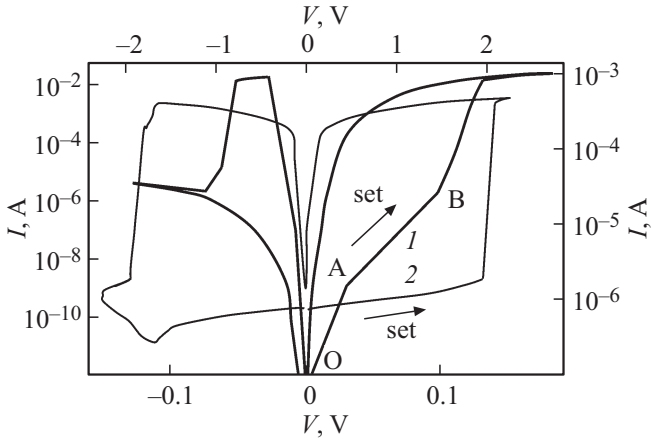

Figure 3. VACs of memristor structures with HP and an electrochemically active silver electrode: *1* — Ag|$CH_3NH_3(Pb)I_{3-x}Cl_x$|FTO (thicker curve), *2* — Ag|$CH_3NH_3(Pb)I_3$|Pt. These VACs are generalizations of sets of characteristics obtained in [11] and [10], respectively. The left and bottom scales correspond to curve *2*, while the right and top scales correspond to curve *1*.

As was already noted, the vacancy density, which changes as $\exp(\varphi_d/T)$ when approaching the cathode, may reach $(10^{20}-10^{21})\,\mathrm{cm}^{-3}$ or even higher values, which are not that lower than the density of halogen atoms in the perovskite lattice. A semiconductor may then be regarded as an amorphous one. For the sake of simplicity, we consider BG narrowing with simultaneous lowering of the conduction band minimum (E_{CBM}) of perovskite, which sets the entry barrier for electrons from a metal. This BG narrowing and variation δE_{CBM} of E_{CBM} as a function of vacancy density N_{vac} may be characterized in a similar way to how it is done in semiconductor theory for variation $\Delta\varepsilon_{\mathrm{F}}$ of the Fermi level position in a doped semiconductor as a function of admixture density N_{adm}: $\Delta\varepsilon_{\mathrm{F}} \propto \ln N_{\mathrm{adm}}$.

It is natural to assume that $\delta E_{\mathrm{CBM}} \to 0$ at $N_{\mathrm{vac}} \to 0$. At the same time, the bandgap becomes irrelevant when the vacancy density approaches a certain limit $N_{\mathrm{vac}}^{\mathrm{up}}$; i. e., $\delta E_{\mathrm{CBM}} \to E_g$. In a regular semiconductor, $N_{\mathrm{vac}}^{\mathrm{up}} \approx \mathrm{DoS}_{\mathrm{CB}}$ (the density of states in the CB); in amorphous perovskite, this limit is significantly higher. Let us assume then that lowering of the CBM (i. e., growth of E_{CBM}) and E_g reduction relative to equilibrium values $E_{\mathrm{CBM}}^{\mathrm{eq}}$, E_g^{eq} in Figure 2, a are in all cases given by

$$E_{\mathrm{CBM}} - E_{\mathrm{CBM}}^{\mathrm{eq}} = \frac{1}{2}\,(E_g^{\mathrm{eq}} - E_g),$$

$$E_g^{\mathrm{eq}} - E_g = \varkappa T \ln\Big(1 + \big(\exp(E_g/\varkappa T) - 1\big)(N_{\mathrm{vac}}/N_{\mathrm{vac}}^{\mathrm{up}})\Big), \qquad (8)$$

where ratio

$$N_{\mathrm{vac}}/N_{\mathrm{vac}}^{\mathrm{up}} = (N_{\mathrm{vac}}^{(0)}/N_{\mathrm{vac}}^{\mathrm{up}})\exp(\varphi/T),$$

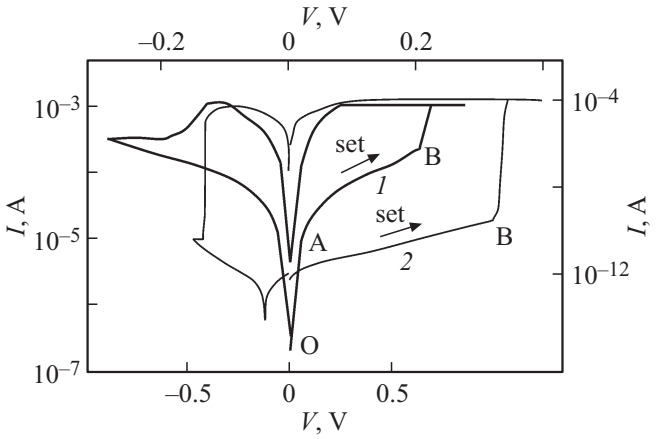

Figure 4. VACs of memristor structures with HP and inert electrodes: *1* — Au|CH_3NH_3(Pb)I_3|ITO (thicker curve), *2* — Au|CH_3NH_3(Pb)$I_{3-x}Cl_x$|FTO. These VACs are generalizations of sets of characteristics obtained in [14] and [15], respectively. The left and bottom scales correspond to curve *1*, while the right and top scales correspond to curve *2*.

$\varkappa$ is a dimensionless parameter that may depend on N_{vac}, but is just a characteristic of perovskite. If $\varkappa$ is constant, a quadratic equation in $\exp(E_g/\varkappa T)$ is obtained at $\varphi = \varphi_d$. Its solution is

$$2\exp(E_g/\varkappa T) = 1 - \xi + \left((1-\xi)^2 + 4\xi\exp(E_g^{\text{eq}}/\varkappa T)\right)^{1/2}, \tag{9}$$

where

$$\xi = \exp(-\varphi_d/T)(N_{\text{vac}}^{(0)}/N_{\text{vac}}^{\text{up}})^{-1}.$$

If φ_d is small,

$$\exp\left((E_g^{\text{eq}} - E_g)/\varkappa T\right) = \exp(\varphi_d/T)(N_{\text{vac}}^{(0)}/N_{\text{vac}}^{\text{up}}), \tag{10}$$

and bandgap narrowing $E_g^{\text{eq}} - E_g \propto \varphi_d$, while current

$$J_e \propto \exp(\varphi_d/T) \propto \exp\left(\frac{1}{2}V/T\right), \tag{11}$$

At large φ_d values,

$$E_g^{\text{eq}} - E_g = E_g^{\text{eq}} - \varkappa T\exp(-\varphi_d/T)(N_{\text{vac}}^{(0)}/N_{\text{vac}}^{\text{up}})^{-1} \times \left(\exp(E_g^{\text{eq}}/\varkappa T) - 1\right),$$

and current saturates as a negative, but still exponential function: $J_e \propto C - \exp(-\varphi_d/T)$. The application of (10) to a point with current potential φ specifies lowering of the CBM level from the cathode interface throughout the entire depth of the near-cathode layer.

Thus, with a slight near-cathode drop $\varphi_d = V/2$, we obtain exponential growth that is faster than power-law growth, but not overexponential (i. e., the one that would resemble resistive switching). This behavior agrees with experimental data on metal|(MA)PbX_3|metal memristors. The VACs in Figures 3 and 4 were plotted based on literature data, since we did not perform experiments with nonmodified HP. The plots in Figures 3 and 4 represent systems with one electrode made from chemically active silver [10–13] and with two chemically passive electrodes [14–16], respectively. Only two typical plots are shown in each figure, since visual clarity is lost when more data are used.

All switchings are clearly bipolar in nature. Therefore, further analysis is limited at the moment to voltages $V > 0$ and the process of setting a high-resistance state (set). It can be seen from Figures 3 and 4 that exponential sections (to the left of point A) coexist with sections spanning from point A to point B (which corresponds to RS) that feature linear or weak power-law growth.

In our view, these sections of slow growth may be characterized completely within the developed concept of ion–vacancy conductivity if one augments it with the analysis of surface states (SS) of the cathode−gap interface. Indeed, a negative SS charge is identical for an external-circuit electron to an additional potential barrier φ_{exc}. An estimate of its height may be obtained by multiplying electrical field F within a metal in a small neighborhood of the SS charge by Fermi radius $r_{\text{F}} = \left(\hbar^2/(2m\varepsilon_{\text{F}}^{\text{cath}})\right)^{1/2}$; field F is specified by the Gaussian law: $(1 + \varepsilon_{\text{PSK}})F = 4\pi\sigma_{\text{SS}}e^2$, where σ_{SS} is the surface charge density and ε_{PSK} is the permittivity of perovskite (PSK).

It is natural to assume that at low voltage, $\sigma_{\text{SS}} \propto$ vacancy density N_{vac} at the cathode: $\sigma_{\text{SS}} \propto (1/a^2)N_{\text{vac}}/N_{\varkappa}^{(0)}$ (a is the lattice constant). The potential drop over distance r_{F} is then on the order of

$$\varphi_{\text{exc}} = \frac{r_{\text{F}}r_1}{a^2}\,\frac{4\pi E_1}{1+\varepsilon_{\text{PSK}}}\,\frac{N_{\text{vac}}^{(0)}}{N_{\varkappa}^{(0)}}\exp\left(\frac{V}{2T}\right), \tag{12}$$

($E_1 = 1\,\text{eV}$, $r_1 = 1.44 \cdot 10^{-7}\,\text{cm}$ are scale parameters of energy and distance), and the associated additional current reduction as a function of voltage is overexponential in nature. It is clear, however, that the introduction of recombination of the SS charge with positive vacancies limits the growth of this charge. Let us assume for illustration purposes that only a single surface state is present. Its electron filling factor $0 < \mu < 1$ is set by the balance between incoming (free) overbarrier electrons with density n_e^f and the SS charge recombination with positive halogen vacancies from within the gap: $n_e^f n_{\text{SS}}^{\max} C_f(1-\mu) = n_{\text{SS}}^{\max} C_{\text{vac}}\mu N_{\text{vac}}$, where $n_{\text{SS}}^{\max}$ is the charge density at this SS at maximum filling and C_f, C_{vac} are constants. Thus, fill factor $\mu = n_e^f C_f/(n_e^f C_f + C_{\text{vac}}N_{\text{vac}})$ at a high vacancy density $\propto 1/N_{\text{vac}}$, and the SS charge and its density σ_{SS} are independent of N_{vac}.

Therefore, the entering current as a function of voltage at a low vacancy density is proportional to

$$\exp\left(\frac{1}{2}V/T - B\exp\left(\frac{1}{2}V/T\right)\right),$$

while the same current at a high vacancy density reaches a certain saturation level. The entire spectrum of surface states with various filling factors specifies kinks of VAC

curves at the level of higher-order derivatives, and VAC sections between these kinks may be regarded as power-law dependences on voltage V with different exponents of power.

This analysis suggests that the shape of the O–A–B section (Figures 3 and 4) of VACs for a metal|perovskite|metal system is natural, but does not reveal the presence of resistive switching. The emergence of filaments with an anomalously high electronic conductivity may be regarded as a mechanism of such switching. In our view, this mechanism is not the only one available and, at the very least, requires clarification. It is normally assumed that filaments grow due to clustering of neutralized ions or neutral vacancies produced in the process of drift of ions or charged vacancies to the corresponding electrode under the influence of a field [1]. In the case of electrochemically active electrodes (Ag), the same mechanism is likely to be implemented in an HP memristor. This is evidenced by the results of measurements of the VAC dependence on the electrode area (specifically, a lack of such dependence in the „ON" state [10–13]). However, no evidence of the formation of individual filaments have been reported for chemically inert electrodes [14–16]. In our view, when the mobilities of vacancies and halogen ions are high, it is natural to seek the cause of RS in a change in the nature of their motion within the gap.

Limiting ourselves to the „vacancy" (near-cathode) half of the gap for illustrative purposes, we may hypothesize the following. Up to a certain voltage across the gap, the field motion of charged vacancies, opposing diffusion motion of the same vacancies from the cathode to the anode, and opposing diffusion motion of vacancies neutralized at the cathode proceed within one and the same corridor. At higher voltages, this motion pattern is hard to maintain for a number of reasons, such as (1) resonance charge exchange of charged vacancies moving to the cathode under a dominant field current component and neutralized vacancies that drift from the cathode (where neutralization takes place) in the opposite direction; (2) similar non-resonance charge exchange of halogen ions X^+ moving to the anode (under a dominant field current) and X_2 molecules drifting from the anode (where neutralization takes place) toward the cathode: $X^- + X_2 \leftrightarrow X + X_2^-$.

Both factors lead to energy losses. With partial separation of the motion of charged components near the cathode and the anode, these losses decrease (at an estimate level, they vanish), and the recovered energy induces the emergence of closed vortices of motion of vacancies (in the cathode part of the gap) and halogens (in the anode part). The gap is then split into Benard-type cells (Figure 5) such that regions dominated by the field (F in Figure 5) and diffusion (Diff) are present in each cell.

Let us estimate the threshold of splitting into cells and their scale while limiting ourselves to the planar vortex geometry (i. e., infinite „waves" in the direction perpendicular to the plane of Figure 5) and to the examination of one half of a vortex from the midplane of the gap to the cathode. The

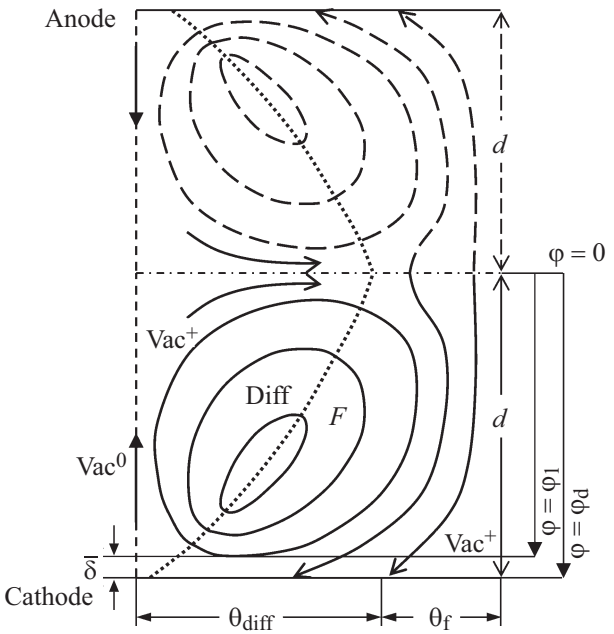

Figure 5. Diagram of one half of a cell containing a vortex in the direction along the electrode surface.

energy dissipation rate associated with the resonance charge exchange of vacancies (prior to splitting into vortices) is

$$Q_{\text{rescharge}} = \sigma_{\text{res}} N^+_{\text{vac}} N^0_{\text{vac}} (v^+_{\text{vac}} + v^0_{\text{vac}}) \Delta E A_{\text{vort}} \qquad (13)$$

with a dimension of W/cm, where A_{vort} is the cross-section area of a cell with a vortex, σ_{res} is the cross section of charge exchange, v^+_{vac}, v^0_{vac} are the magnitudes of velocities of charged and neutral vacancies moving toward each other, upper indices „+" and „0" of N_{vac}, v_{vac} indicate the vacancy charge, and ΔE is the energy lost in charge exchange. Notably, $v^+_{\text{vac}} \ll v^0_{\text{vac}}$, since v^0_{vac} is governed by diffusion only, while field and diffusion currents are balanced in v^+_{vac}.

Vortex currents produce two contributions to the dissipation rate. The first is Joule heat generated by the vortex current

$$Q^{(1)}_{\text{vort}} \sim \frac{U^2}{R} \sim \frac{\mu e}{L} A \left(U - T \frac{\delta N}{N} \right)^2, \qquad (14)$$

where U, R, L, A are the nominal values of voltage, resistance, length, and transverse size of a plane current tube and δN and N are the material density difference and the absolute value of this density. The same quantity in the conditions of the discussed problem written as a function of current of charged vacancies and their velocity is

$$Q^{(1)}_{\text{vort}} = \frac{e N^+_{\text{vac}}}{\mu^+_{\text{x}}} \int_0^G (v^+_{\text{vac}})^2 (r) 2\pi r dr, \qquad (15)$$

where G is the outer vortex radius and r is a variable radial coordinate of integration within a vortex. With a linear dependence of velocity on radius,

$$v^+_{\text{vac}}(r) = v^+_{\text{vac}} r / G, \qquad (16)$$

$$Q_{\text{vort}}^{(1)} = (eN_{\text{vac}}^{+}/\mu_{x}^{+})\left(\pi(v_{\text{vac}}^{+})^2G^2/2\right). \quad (17)$$

With any other power law of velocity growth from the core of a vortex to its outer radius, only the coefficient in the denominator in (17) changes, which is insignificant at an estimate level.

The second contribution to dissipation in a vortex is produced by viscosity, although this concept has a clear meaning only at $N_{\text{vac}}^{+} \sim N_{x}^{+}$ (i.e., within small fraction χ of a vortex). By analogy with (15), the corresponding dissipation rate is

$$Q_{\text{vort}}^{(2)} = \frac{\eta}{2}\int_{0}^{G}\left(\frac{\partial v_{\text{vac}}^{+}}{\partial r}\right)^2(r)2\pi r dr. \quad (18)$$

With a linear velocity reduction in the radial direction (16),

$$Q_{\text{vort}}^{(2)} = \pi\eta(v_{\text{vac}}^{+})^2/2 \quad (19)$$

does not depend on vortex radius G.

It follows from (13), (17), and (19) that the energy saved by virtue of resonance charge exchange is sufficient for vortex „spinup“ if

$$\sigma_{\text{res}}N_{\text{vac}}^{+}N_{\text{vac}}^{0}(v_{\text{vac}}^{+}+v_{\text{vac}}^{0})\Delta E A_0 > \frac{eN_{\text{vac}}^{+}}{\mu_{X}^{+}}\frac{\pi(v_{\text{vac}}^{+})^2G^2}{2} + \frac{\pi\eta(v_{\text{vac}}^{+})^2}{2}. \quad (20)$$

Since $v_{\text{vac}}^{+} \ll v_{\text{vac}}^{0}$, we obtain the following by discarding the viscous term, which is hard to incorporate, and under the assumption that $\Delta E = m_X(v_{\text{vac}}^{+})^2/2$:

$$\sigma_{\text{res}}N_{\text{vac}}^{+}N_{\text{vac}}^{0}v_{\text{vac}}^{0}\, m_X(v_{\text{vac}}^{0})^2 > \frac{eN_{\text{vac}}^{+}}{\mu_{X}^{+}}(v_{\text{vac}}^{+})^2.$$

A slight modulation of velocity in the strongly nonlinear term on the left-hand side makes the formation of vortices possible. If we equate roughly the fluxes of charged and neutral vacancies taking into account the balance of these fluxes at the cathode, the vortex spinup condition is

$$\sigma_{\text{res}}N_{\text{vac}}^{+}\, m_X(v_{\text{vac}}^{0})^2 > v_{\text{vac}}^{+}e/\mu_{X}^{+}. \quad (21)$$

Apart from velocities, all parameters in this expression depend only weakly on the voltage across the gap. However, the velocity of neutral vacancies is squared on the left-hand side of (21), while the velocity of charged vacancies on the right-hand side is not. These velocities differ drastically in magnitude, but have similar functional dependences on voltage. Therefore, threshold values of each velocity (and, consequently, the parameter gradients within the gap) should exist. A threshold value of the potential gradient allows one to reconstruct the threshold of the overall voltage across the gap.

Velocity v_{vac}^{0} is specified by variation $(N_{\text{vac}}^{0})_{\text{diff}} - (N_{\text{vac}}^{0})^{(0)}$ of the densities of neutral vacancies in region D over vortex length $d-\bar{\delta}$ from the cathode to the middle of the gap, where $\bar{\delta}$ is the width of a narrow boundary layer at the cathode and $(N_{\text{vac}}^{0})_{\text{diff}}$, $(N_{\text{vac}}^{0})^{(0)}$ are the densities of neutral vacancies at the boundary of this layer in the diffusion part of a vortex (Diff region). Velocity v_{vac}^{+} depends on similar difference $(N_{\text{vac}}^{+})_{\text{diff}} - (N_{\text{vac}}^{+})^{(0)}$ and potential drop φ_1 in the field region of a vortex. As an estimate, we may set the gradients of densities and potentials to be equal to derivatives in the midplane of the gap

$$v_{\text{vac}}^{0} = \mu_{X}^{0}(\varphi_0'/T);\;\; v_{\text{vac}}^{+} = v_{\text{vac}}^{0}\left(J_e/(\mu_{X}^{0}e(N_{\text{vac}}^{0})^{(0)}\varphi_0')\right). \quad (22)$$

Limiting ourselves to ohmic dissipation and setting cross section $\sigma_{\text{res}} = 10^{-14}\,\text{cm}^2$, we then determine the threshold voltage across the gap at a level of several tenths of B, which agrees in order of magnitude with the experimental value.

The characteristic size of a vortex may be estimated by equating the carrier current to the electrode in region F within a vortex, the carrier current from the electrode into the gap in region Diff, and the current along the cathode in transition from one region to the other. In the order of magnitude, vortex current I_{vort} is then

$$\begin{aligned} I_{\text{vort}} &= \frac{\mu_{X}^{+}\theta_f}{d-\delta}(N_{\text{vac}}^{+})^{(0)}\left(\varphi_1 - T\frac{(N_{\text{vac}}^{+})_f - (N_{\text{vac}}^{+})^{(0)}}{(N_{\text{vac}}^{+})^{(0)}}\right) \\ &= \frac{\mu_{X}^{+}\theta_{\text{diff}}}{d-\delta}(N_{\text{vac}}^{+})^{(0)}\left(T\frac{(N_{\text{vac}}^{+})_{\text{diff}} - (N_{\text{vac}}^{+})^{(0)}}{(N_{\text{vac}}^{+})^{(0)}} - \varphi_1\right) \\ &= \frac{\mu_{X}^{+}\bar{\delta}}{\theta}\langle N_{\text{vac}}^{+}\rangle T\frac{(N_{\text{vac}}^{+})_{\text{diff}} - (N_{\text{vac}}^{+})_f}{(N_{\text{vac}}^{+})^{(0)}}, \end{aligned} \quad (23)$$

which implies that the square of the average extent of field and diffusion regions along the cathode is $\bar{\theta}^2 \sim 2\bar{\delta}(h-\bar{\delta})$ and the vortex structure period along the cathode is $4\left(2\bar{\delta}(h-\bar{\delta})\right)^{1/2}$ (in Figure 5, $\bar{\theta} \approx (\theta_{\text{diff}}+\theta_f)/2$ and $\bar{\delta}$ is indicated as a certain average value for both regions).

The discussed mechanism differs substantially both from the emergence of fairly random filaments and from the mechanism that is associated in literature with a change in the Schottky barrier and evolves uniformly over the entire electrode surface. In the considered system, the Schottky barrier itself exerts almost no influence on current transport. At the same time, it is very hard to envision a system that features a gigantic size ratio of electrodes to the gap with processes evolving uniformly throughout the entire surface area. Therefore, the proposed mechanism appears to be natural.

Having matched the experimental VACs in Figures 3 and 4 with the cell pattern, one may assume that RS at point B is the emergence of cells. However, as long as the results of detailed calculations remain unavailable, it is equally probable that the emergence of cells is associated with the VAC kink at point A. A modulated pattern of regions of dominance of neutral vacancies then forms on the cathode surface around point A. Some of these vacancies remain on the surface, initiating the growth of a whole system of filament seeds when the voltage increases. However, at a high mobility of ions and vacancies, bridging of a single filament with a moderate electronic conductivity

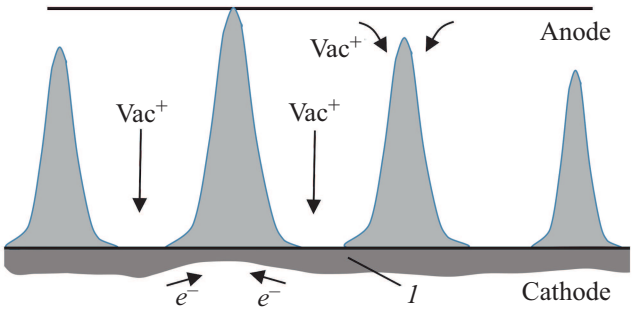

Figure 6. Diagram of influence of filaments of neutral vacancies with electronic conductivity on the SS of the cathode–HP interface. *1* — Provisional distribution of the SS charge density at the cathode.

does not alter the current flow pattern radically. Instead, the flow of electrons to a filament from surface states in the surrounding regions (Figure 6) lowers the effective barrier to electron propagation from a metal to the cathode–gap interface.

This is illustrated in Figure 6 as narrowing of dark band *1* that corresponds to the SS charge. Barrier lowering acts as an element of positive feedback: increased inflow of electrons from a metal to the interface — increased inflow of charged vacancies to the cathode — enhanced surface density of neutral vacancies — faster growth of neighboring filaments. This multiple-filament mechanism also implies proportionality of the „ON" current to the area, which agrees with the results of an experiment with inactive electrodes [14–16].

3. Conclusion

Hybrid perovskites are specific in having a low activation energy of escape of system components and their migration in an electrical field. This is especially true for halogen ions. As a result, this system assumes the properties of ion–vacancy plasma with a high charge density (on the order of $10^{18}-10^{19}\,\mathrm{cm}^{-3}$) and a high velocity of migration of ions and vacancies. Therefore, it seems unlikely that RS is caused by the formation of nanofilaments of a certain composition. With intense migration of components, the volt–ampere characteristics should have a near-exponential shape. This agrees with experimental data, but not within all VAC sections outside of RS points. In other sections, the shape of these characteristics, which are close to weak power-law dependences, may be characterized with the introduction of surface states within the same model of exclusively ion–vacancy gap conduction (i. e., without electrons).

The HP gap structure in this model allows for switching by splitting the gap space into vortex motions of ions and vacancies of the Benard cell type. The characteristic scale and the formation threshold of such cells were estimated. It was demonstrated that cells may act as a preparatory stage to splitting of the HP space into a multitude of closely spaced filaments, which are formed by neutral halogen vacancies and support electronic gap conduction (in addition to the ionic one).

The dynamics of vortex formation and the positioning of regions of vortex motion and filamentary conduction in VACs warrant further study and will be examined in future calculations. The experimental identification of these modes is a no less important task.

Conflict of interest

The authors declare that they have no conflict of interest.

References

[1] F. Pan, S. Gao, C. Chen, C. Song, F. Zeng. Mater. Sci. Eng. **83**, 1 (2014).
[2] D. Cooper, C. Baeumer, N. Bernier, A. Marchewka, C. La Torre, R.E. Dunin-Borkowski, S. Menzel, R. Waser, R. Dittmann. Adv. Mater. **29**, *23*, 1700212 (2017).
[3] A.N. Mikhaylov, E.G. Gryaznov, A.I. Belov, D.S. Korolev, A.N. Sharapov, D.V. Guseinov, D.I. Tetelbaum, S.V. Tikhov, N.V. Malekhonova, A I. Bobrov, D.A. Pavlov, S.A. Gerasimova, V.B. Kazantsev, N.V. Agudov, A.A. Dubkov, C.M.M. Rosário, N.A. Sobolev, B. Spagnolo. Phys. Status Solidi C **13**, *10–12*, 870 (2016).
[4] C. Eames, J.M. Frost, P.R.F. Barnes, B.C. O'Regan, A. Walsh, M. Saiful Islam. Nature Commun. **6**, *1*, 7497 (2015).
[5] A. Walsh, D.O. Scanlon, S. Chen, X.G. Gong, S.-H. Wei. Angewandte Chem. **54**, *6*, 1791 (2015).
[6] F.A. Kröger. The Chemistry of Imperfect Crystals. 2nd ed. North-Holland, Amsterdam (1974). V. 2.
[7] F. Zheng, L.Z. Tan, S. Liu, A.M. Rappe. Nano Lett. **15**, *12*, 7794–800 (2015).
[8] T. Leijtens, S.D. Stranks, G.E. Eperon, R. Lindblad, E.M.J. Johansson, I.J. McPherson, H. Rensmo, J.M. Ball, M.M. Lee, H.J. Snaith. ACS Nano **8**, *7*, 7147 (2014).
[9] X. Guan, W. Hu, M.A. Haque, N. Wei, Z. Liu, A. Chen, T. Wu. Adv. Funct. Mater. **28**, *3*, 1704665 (2018).
[10] E. Yoo, M. Lyu, J.-H. Yun, C. Kang, Y. Choi, L. Wang. J. Mater. Chem. C **4**, *33*, 7824 (2016).
[11] J. Choi, S. Park, J. Lee, K. Hong, D.-H. Kim, C.W. Moon, G.D. Park, J. Suh, J. Hwang, S.Y. Kim, H.S. Jung, N.-G. Park, S. Han, K.T. Nam, H.W. Jang. Adv. Mater. **28**, *31*, 6562 (2016).
[12] X. Zhu, J. Lee, W.D. Lu. Adv. Mater. **29**, *29*, 1700527 (2017).
[13] J.M. Yang, S.G. Kim, J.Y. Seo, C. Cuhadar. Adv. Electron. Mater. **4**, *9*, 21800190 (2018).
[14] C. Gu, J.-S. Lee. ACS Nano **10**, *5*, 5413 (2016).
[15] F. Zhou, Y. Liu, X. Shen, M. Wang, F. Yuan, Y. Chai. Adv. Funct. Mater. **28**, *15*, 1800080 (2018).
[16] B. Hwang, J.-S. Lee. Adv. Mater. **29**, *29*, 1701048 (2017).

Translated by D.Safin